nature publishing group
Open
ARTICLES
ADIPOCYTE BIOLOGY

Cafeteria Diet Is a Robust Model of Human Metabolic Syndrome With Liver and Adipose Inflammation: Comparison to High-Fat Diet

Brante P. Sampey[1], Amanda M. Vanhoose[2], Helena M. Winfield[3], Alex J. Freemerman[1], Michael J. Muehlbauer[3], Patrick T. Fueger[4], Christopher B. Newgard[3] and Liza Makowski[1]

Obesity has reached epidemic proportions worldwide and reports estimate that American children consume up to 25% of calories from snacks. Several animal models of obesity exist, but studies are lacking that compare high-fat diets (HFD) traditionally used in rodent models of diet-induced obesity (DIO) to diets consisting of food regularly consumed by humans, including high-salt, high-fat, low-fiber, energy dense foods such as cookies, chips, and processed meats. To investigate the obesogenic and inflammatory consequences of a cafeteria diet (CAF) compared to a lard-based 45% HFD in rodent models, male Wistar rats were fed HFD, CAF or chow control diets for 15 weeks. Body weight increased dramatically and remained significantly elevated in CAF-fed rats compared to all other diets. Glucose- and insulin-tolerance tests revealed that hyperinsulinemia, hyperglycemia, and glucose intolerance were exaggerated in the CAF-fed rats compared to controls and HFD-fed rats. It is well-established that macrophages infiltrate metabolic tissues at the onset of weight gain and directly contribute to inflammation, insulin resistance, and obesity. Although both high fat diets resulted in increased adiposity and hepatosteatosis, CAF-fed rats displayed remarkable inflammation in white fat, brown fat and liver compared to HFD and controls. In sum, the CAF provided a robust model of human metabolic syndrome compared to traditional lard-based HFD, creating a phenotype of exaggerated obesity with glucose intolerance and inflammation. This model provides a unique platform to study the biochemical, genomic and physiological mechanisms of obesity and obesity-related disease states that are pandemic in western civilization today.

Obesity (2011) **19,** 1109–1117. doi:10.1038/oby.2011.18

INTRODUCTION

In the United States, obesity has recently reached pandemic levels for a variety of reasons including inactivity and poor diet (1,2). The most recent National Health and Nutrition Examination Survey (NHANES) showed that 68.3% of those studied were considered overweight (BMI ≥25) and 33.9% were obese (BMI ≥30) (1). Childhood obesity is particularly important as more children are developing what were previously considered adult diseases, like type II diabetes, high blood pressure, elevated serum insulin and dyslipidemia; with obese children often progressing to obese adults (2,3).

Genetic models of obesity, such as *ob/ob* mice, *db/db* mice, Zucker *fa/fa* obese rats, Agouti yellow mice, and melanocortin 4 receptor knockout mice, have contributed significantly to the understanding of genetic anomalies underlying mechanisms that control energy homeostasis (4). Other investigations into the aberrant homeostasis responsible for most human obesity were carried out using rodent models of diet-induced obesity (DIO) through the administration of high-fat diets (HFD) (4). Traditionally, these diets consist of a simple exchange of carbohydrate-derived calories with fat-derived calories when compared to low fat or chow control diets. However, another experimental rodent diet model exists that more accurately reflects the variety of highly palatable, energy dense foods that are prevalent in Western society and associated with the current obesity pandemic: the "cafeteria diet" (CAF) (5,6). In this model, animals are allowed free access to standard chow and water while concurrently offered highly palatable, energy dense, unhealthy human foods *ad libitum*. This diet promotes voluntary hyperphagia that results in rapid weight gain, increases fat pad mass and prediabetic parameters such as glucose and insulin intolerance (7–10). Moreover, this diet

[1]Department of Nutrition, Gillings School of Global Public Health, School of Medicine; University of North Carolina at Chapel Hill, Chapel Hill, North Carolina, USA; [2]Department of Molecular Physiology and Biophysics, Vanderbilt University Medical Center, Nashville, Tennessee, USA; [3]Sarah W. Stedman Nutrition and Metabolism Center, Department of Pharmacology and Cancer Biology, Duke University Medical Center, Durham, North Carolina, USA; [4]Department of Pediatrics and Cellular and Integrative Physiology, Indiana University School of Medicine, Indianapolis, Indiana, USA. Correspondence: Liza Makowski (liza.makowski@unc.edu)

Received 3 September 2010; accepted 9 January 2011; published online 17 February 2011. doi:10.1038/oby.2011.18

engages hedonic feeding, consistent with the observed voluntary hyperphagia, which produces long-lasting neuronal alterations predicted to underlie non-homeostatically regulated feeding behaviors associated with some forms of human obesity (11,12). Current US Department of Agriculture labeling requirements combined with meticulous laboratory record keeping enables a research model of DIO that models progression to insulin resistance and diabetes.

To date, however, direct comparisons between the CAF model and other DIO animal models have not been adequately evaluated. Therefore, we embarked on a comprehensive comparative study, which demonstrated that the CAF diet is a more robust model for human obesity compared to HFD. Our hypothesis was that CAF diet would be a more representative model of human metabolic syndrome; indeed, we provide supportive evidence of severe obesity, nonalcoholic steatohepatitis (NASH), and glucose intolerance compared to a traditional lard-based HFD. In addition, as the role of chronic low-grade systemic inflammation is increasingly recognized to play a part in metabolic syndrome, we demonstrated dramatic CAF-induced inflammation in liver and white and brown adipose tissues (BAT). Use of this rapid and potent CAF DIO model may be useful to identify novel pathways for preventative intervention or therapeutics in the treatment of human obesity.

METHODS AND PROCEDURES

Animals

Male Wistar rats (~200 g, 7–8 weeks old) (Harlan Laboratories, Dublin, VA) were housed 2 rats/cage in a 12 h light/dark cycle and acclimated to the Duke animal housing facility on *ad libitum* undefined standard chow 7001 ("SC," Harlan Teklad) for 2 weeks before assignment to one of four experimental diet groups. Upon initiation of experimental diets, rats (avg. 300 g, 9–10 weeks old) were either maintained on *ad libitum* SC as controls or switched to *ad libitum* defined 45% fat chow ("HFD," Research Diets D06011802), the matched low-fat chow control (low-fat diet (LFD) Research Diets D07010502), or provided a CAF with three human snack foods varied daily in addition to *ad libitum* SC (see **Supplementary Table S1** online). The CAF diet foods included cookies, cereals, cheese, processed meats, crackers, etc. and were provided in excess (see **Supplementary Table S2** online). Snack items were weighed before and after consumption, corrected for drying, and varied daily according to the fat, protein, and carbohydrate content as listed in **Supplementary Table S2** online. Fat intake was the largest macronutrient alteration in CAF rats, however, simple carbohydrate consumption was also elevated over HFD and SC rats groups. There are no added sugars to the SC diet; any sugars present are derived from whole-grains (corn, oats, etc.). The manufacturer Harlan Teklad estimates that simple sugars are <5% of total carbohydrates in SC7001. It should be noted that the LFD-fed rats also consumed the most simple sugars as a result of sucrose substitution for fat in the diet formula (see **Supplementary Table S3** online).

Two experimental groups of SC and CAF-fed rats (n = 8–9 per diet per group) along with one experimental group of SC, LFD, and HFD-fed rats (n = 8 per diet) were initiated in parallel overlapping by 4–6 weeks. Food consumption and weight gain was monitored daily for 10 weeks (**Figure 1a–d**) to carefully characterize food intake on CAF diet. A subsequent group of experimental animals (n = 8–10 per diet) were fed the four respective diets for 15 weeks and analyzed for glucose tolerance, insulin sensitivity, metabolic alterations, and tissue mRNA, metabolite and phenotypic analysis (**Figures 1e,f,2,3,4,5,6,** and **7,** **Supplementary Figures S1** and **S2** online). Nonesterified fatty acids in plasma were measured enzymatically (Wako, Richmond, VA) using the Hitachi 911 clinical chemistry analyzer (Hitachi, Tokyo, Japan).

GTT and ITT

For 1 week prior to the glucose tolerance test (GTT) or insulin-tolerance test (ITT), animals were acclimated daily to the procedure room and handling for injections and blood draws. Rats were fasted overnight (16 h) and a basal blood draw from the saphenous vein was collected for plasma glucose and insulin measurements 1 h before glucose administration. The GTT was performed after 7 weeks on respective diets; rats were given an intraperitoneal injection of glucose (1 g/kg of body weight; 45% glucose). Blood was obtained from the tail vein via nick immediately before glucose injection and every 30 min thereafter for a period of 180 min, and glucose levels were measured with BD Logic Glucose Meter (Becton-Dickinson, Franklin Lakes, NJ). ITT was performed after 11 weeks where rats were given an intraperitoneal injection of insulin (0.75 IU/kg body weight; Humulin Regular; Eli Lilly, Indianapolis, IN) and blood glucose was measured as in GTT. The homeostasis model assessment was used to calculate approximate insulin resistance (glucose (mg/dl) × insulin/405) (13–16). Plasma insulin was measured with a mouse insulin enzyme-linked immunosorbent assay (Millipore, Billerica, MA).

Tissue collection

After 15 weeks of experimental diet, food was removed for 4–6 h before sacrifice under nembutal anesthesia for tissue collection. Cardiac blood was collected and divided into plasma (1.5 ml blood + 10 µl 1.7 mg/ml EDTA) and serum (clotted for 2 h at room temperature) aliquots, collecting the supernatant fractions after centrifugation (3,800*g*, 10 min, 4 °C). Pancreas, liver, epididymal white adipose tissue (eWAT), and BAT were rapidly isolated, washed in ice-cold phosphate-buffered saline, patted dry and weighed before freeze clamping and snap freezing in liquid nitrogen. A portion of eWAT, BAT, liver, and pancreas was placed in a cassette and fixed in Bouin's fixative overnight, washed with 70% ethanol, and paraffin-embedded for histologic analysis. The remaining portion of the eWAT fat pads was digested to obtain the stromal-vascular fraction (SVF) (17). Briefly, tissue was immediately immersed into 25 mmol/l HEPES-buffered Dulbecco's modified Eagle's medium supplemented with 1% fatty acid free low endotoxin BSA (A8806; Sigma-Aldrich, St Louis, MO), and minced into <10 mg pieces, and filtered through nylon mesh. An lipopolysaccharide-depleted collagenase cocktail (Liberase 3; Roche Diagnostics, Indianapolis, IN) at a concentration of 0.03 mg/ml with 0.2 mg/ml DNAse I (Sigma-Aldrich) was added to each tissue filtrate. The samples were incubated in a shaking water bath at 37 °C for 20–30 min. Once digestion was complete, samples were passed through 250-µm nylon mesh (Sefar, Depew, NY). The suspension was centrifuged at 200*g* for 5 min to pellet the SVF. The SVF was isolated after lysing red blood cells and a final spin to remove liquid.

Histology

Paraffin-embedded tissues were sectioned at 5 microns and mounted for histological staining. Fixative was removed using a graduated series of xylenes (Sigma, St Louis, MO), tissues were rehydrated and then flushed for an additional 15 min in deionized water to remove any remaining fixative. Tissue sections were stained using Harris hematoxylin and eosin (H&E) staining or prepared for immunostaining of adjacent serial sections. Briefly, immunohistochemisty was carried out using serial sections corresponding to H&E-stained tissue sections, processed for heat-induced epitope-retrieval using the Dako Target Retrieval Solution in conjunction with Dako PT Link (Dako North America, Carpinteria, CA). Samples were washed once in Tris-buffered saline/Tween 20 and then exposed to 3% hydrogen peroxide to ablate the innate peroxidase activity of the tissue. Tissues were then blocked in a commercial protein blocking solution (Dako, X0909) and exposed to primary antibodies at 4 °C overnight with gentle agitation (1:250). The sections were washed three times in Tris-buffered saline/Tween 20

for 15 min each. Biotinylated secondary antibody was added for 1 h at room temperature (1:500), and the tissues washed. Visualization of the target epitopes recognized by primary and secondary antibody interactions were established using an avidin/biotinylated horseradish peroxidase kit (Vectastain Elite ABC; Vector Laboratories, Burlingame, CA; PK6100, 1:50) incorporating DAB as the chromogen. The primary antibodies used were raised against macrophage markers F4/80 (Santa Cruz, Santa Cruz, CA, sc-25830, 1:100) and CD163 (AbD Serotech, Raleigh, NC, 1:100), and the tissue sections briefly counterstained with Harris hematoxylin to highlight tissue architecture and nuclear location. Digital photomicrographs of stained tissues were captured using a Nikon Eclipse TS100 equipped with a digital camera using TSView7 software, Version 6.0.2.1 (Tucsen Imaging Technology, Fujian, China).

Pancreatic islets of Langerhans were visualized by performing immunohistochemistry with an insulin antibody. Briefly, paraffin-embedded sections of pancreata were deparaffinized, rehydrated, quenched of endogenous peroxidase activity, blocked, incubated with rabbit anti-anti-insulin primary antibody (Santa Cruz) overnight at 4 °C, and incubated with ImmPRESS reagent (peroxidase conjugated anti-rabbit Ab; Vector Laboratories) for 30 min NovaRed (Vector Laboratories) was used as the substrate for colorimetric detection. Sections were lightly counterstained with hematoxylin. Images were acquired using an Axio-Observer Z1 microscope (Zeiss, St Louis, MO) fitted with an AxioCam HRC camera and operated with Axio-Vision Software, v. 4.8 (Zeiss). Representative images for each tissue (eWAT, liver, BAT, pancreas) from each treatment group were selected. To determine the inflammatory state of the eWAT, three randomly selected 10× fields were assessed for crown-like structures (CLS) from both H&E stain and F4/80 macrophage staining, per study animal. Liver inflammation was determined by enumerating the inflammatory loci per 10× field using three fields H&E and three fields F4/80 stained for each animal (randomly selected). Data are presented as the mean ± s.e.m. for each treatment group.

RNA isolation

QIAzol Lysis Reagent was used to isolate mRNA from snap-frozen SVF pellets with DNAse treatment (RNeasy Lipid Tissue Mini Kit mRNA; Qiagen, Valencia, CA). Samples were isolated in duplicate on two columns and eluted into the same tube. mRNA quantity and quality were analyzed by Nanodrop (Thermo Scientific, Wilmington, DE) and Bioanalyzer 2100 (Agilent, Wilmington, DE), respectively. For quantitative PCR analysis, cDNA was synthesized using IScript (Bio-Rad, Hercules, CA). Real-time quantitative PCR was completed using the Roche LightCycler 480 using LightCycler 480 SW 1.5 software and TaqMan Assay on Demand primers for tumor necrosis factor α (Applied Biosystems, Carlsbad, CA).

Statistics

Data are shown as means ± s.e.m. Analysis was performed using ANOVA followed by a Tukey–Kramer honestly significant difference, and when appropriate a two-tailed Student's *t*-test $P < 0.05$ using JMP (SAS Institute, Cary, NC).

RESULTS

CAF diet-induced hyperphagia and weight gain

Prior to the start of the study, there were no differences in food intake or body weight between animals assigned to experimental diet groups. We first evaluated food intake, fat intake, and body weight changes in male Wistar rats fed four different diets (Figure 1 and **Supplementary Table S1** online): (i) "SC": control rats were continued on standard chow (SC7001) fed from birth, which contains ~12% kcal derived from fat (porcine fat and linoleic acid); (ii) "CAF": continued SC7001 access plus a daily assortment of three human snack items; (iii) "LFD": a defined standard chow (SC502) with 10% kcal derived from fat (lard and soybean oil); (iv) "HFD"-matched to SC502 with decreased carbohydrate content and increased lard content (45% kcal derived from fat). Rats on the CAF diet consumed standard chow at ~15% of that consumed by rats fed standard chow only.

Average weekly nutrient intake per rat in a 10-week food intake study is summarized in **Supplementary Table S3** online. All rats consumed ~100 kcal/day/rat except for CAF-fed rats who significantly consumed about 30% more calories (**Supplementary Table S3** and Figure 1a). HFD-fed rats, unlike CAF-fed rats, significantly decreased total gram intake

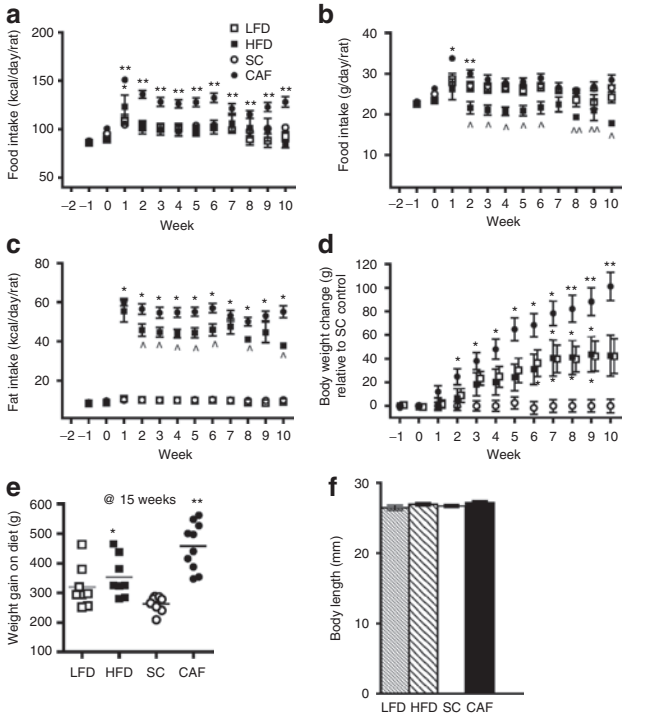

Figure 1 Cafeteria diet (CAF) drives food and fat consumption. (**a**) Male Wistar rats on CAF have elevated food intake in terms of kcal compared to standard chow (SC) control, high-fat diet (HFD), and low-fat diet (LFD). (*HFD $P < 0.05$ vs. all; **CAF $P < 0.0001$ vs. all). (**b**) Upon initiation of diets, only HFD-fed rats decreased food intake in grams (g) with an acute increase in CAF-intake. (*CAF $P < 0.005$ vs. all; ** CAF $P < 0.005$ vs. SC and HF; ^HF $P < 0.005$ vs. all; ^^HF $P < 0.005$ vs. SC and CAF). (**c**) CAF-fed rats consume more fat when compared to animals receiving HFD, LFD, or SC. (*CAF and HF $P < 0.001$ vs. SC and LF; ^CAF $P < 0.05$ vs. HF). (**d**) CAF-diet fed rats exhibited significant weight gain starting at 2 weeks and persisting throughout the study. Data are normalized to SC. (*CAF, LFD, or HFD $P < 0.05$ vs. SC, **CAF $P < 0.05$ vs. SC). (**e**) After 15 weeks on diet, CAF-fed rats exhibited greater total weight gain when compared to SC, LFD, and HFD. Although HFD-fed rats also gained weight, there is no difference in the weight gain between the HFD and LFD groups, however weight gain did reach statistical significance when compared to the SC control group. (*HF $P < 0.05$ vs. SC; **CAF $P < 0.05$ vs. all). (**f**) There were no changes in body length after 15 weeks on diet. (**a**–**d**) were conducted on a set of rats fed diet for 10 weeks. ($n = 23$–24, SC, $n = 8$ LFD, HFD, $n = 17$ CAF) and (**e**,**f**) were conducted on a group of rats fed diet for 15 weeks ($n = 8$, SC, LFD, and HFD, $n = 10$ CAF).

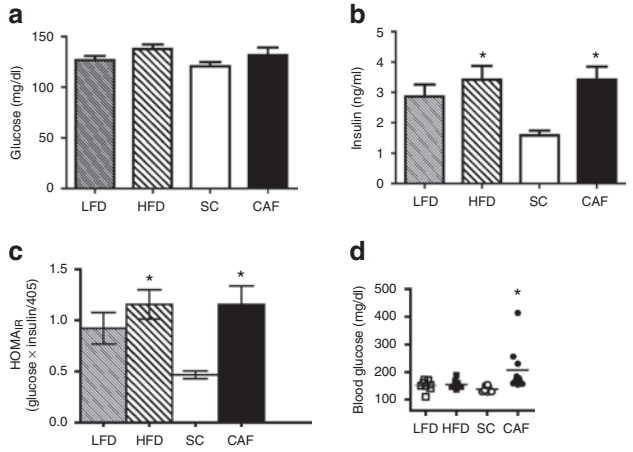

Figure 2 Cafeteria diet (CAF)-fed rats displayed hyperglycemia and hyperinsulinemia. Insulin sensitivity was evaluated on rats at weeks 7 and 11 during the 15-week study. (**a**,**b**) Fasting glucose levels were not different at 7 weeks of age while only standard chow (SC)-fed rats maintained low insulin levels, which were significantly different than CAF- and high-fat diet (HFD)-fed rats. (**c**) Homeostasis model assessment of insulin resistance (HOMA$_{IR}$) calculations at 7 weeks on diets indicated that CAF and HF groups demonstrated statistically significant elevations in insulin resistance compared to SC-fed rats. (*P < 0.05 vs. SC). (**d**) CAF-fed rats had significantly elevated blood glucose after a 6 h light cycle fast at 15 weeks on diet (time of sacrifice) compared to SC, while low-fat diet (LFD) and HFD maintained normal glucose levels. (n = 8, SC, LFD, and HFD, n = 10 CAF). (*P < 0.05 SC to CAF).

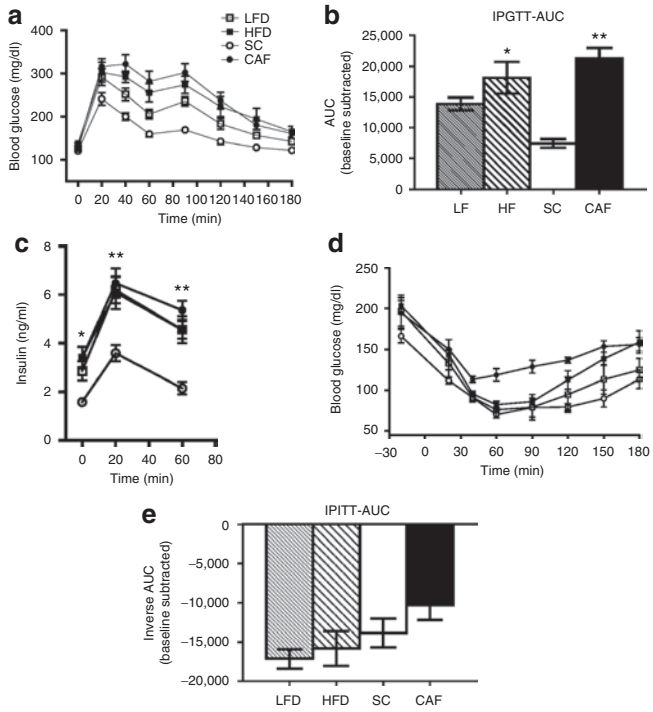

Figure 3 Cafeteria diet (CAF)-fed rats became glucose intolerant. (**a**) Rats fed low-fat diet (LFD) and high-fat diet (HFD) maintained similar tolerance to glucose when challenged with intraperitoneal glucose tolerance tests (IP-GTT) at 7 weeks on diets. (**b**) Area under the curve (AUC) quantifications for IP-GTT of averaged individual animals showed CAF-fed rats developed significant glucose intolerance compared to the standard chow (SC)-fed controls. (*P < 0.05 vs. SC; **P < 0.05 vs. SC and LF). (**c**) Insulin levels measured during IP-GTT at 11 weeks on diets revealed that all animals induced insulin secretion in response to glucose injections, however, SC-fed rats had lower basal insulin levels and maintained low insulin levels during the IP-GTT when compared to the other diet exposed groups. (*P < 0.05 CAF and HF vs. SC; **P < 0.05 all vs. SC; n = 8, SC, LFD, and HFD, n = 10 CAF). (**d**) Intraperitoneal insulin-tolerance tests (IP-ITT) revealed blunted insulin action in CAF-fed rats challenged with 0.7 IU/kg insulin when compared to SC-fed rats, but there were no significant differences between diets. HFD-fed and LFD control-fed rats displayed an intermediate insulin response that did not vary significantly between these groups. (**e**) AUC quantifications for IP-ITT of individual animals averaged. (n = 4, SC, LFD, and HFD, n = 5 CAF).

of the calorically dense diet to normalize caloric consumption by week 2, an effect commonly seen in rodents placed on HFD (**Figure 1b**). Fat intake consumption paralleled percent fat content of diet with SC and LFD consuming ~10 kcal/day/rat, the HFD group at 45 kcal/day/rat, and the CAF-diet group at 55 kcal/day/rat (**Figure 1c**). CAF-fed rats gained the most weight on the diet, almost double the weight gain evident in SC controls, whereas LFD and HFD-fed rats demonstrated similar and intermediate weight gain (**Figure 1d**). A subsequent group was placed on the four experimental diets for 15 weeks, demonstrating similar and continued weight gain (**Figure 1e** and **Supplementary Figure S1** online) with no statistical differences in body length among treatment groups (**Figure 1f**).

CAF-diet induced hyperglycemia and insulin resistance

At an intermediate time point (7 weeks) on diets, glucose homeostasis was maintained irrespective of diet, as blood glucose measured in obese and lean rats fasted overnight was not significantly different amongst the four diet groups (**Figure 2a**). However, insulin was approximately doubled in CAF- and HFD-fed rats compared to SC controls (**Figure 2b**). Consistent with the observed intermediate body weight phenotype, LFD-fed rats displayed a modest, nonsignificant elevation in fasting insulin compared to SC. Similarly, homeostasis model assessment of insulin resistance HOMA$_{IR}$ calculations as a measure of insulin sensitivity indicated that CAF- and HFD-fed rats were twofold less insulin sensitive than SC controls at just 7 weeks into the diets (**Figure 2c**). After extended exposure to diets (15 weeks), hyperglycemia became evident in CAF-fed rats only, as 3 of 10 exhibited hyperglycemia after a 6 h fast before sacrifice with no differences between LFD, HFD, and SC control groups (**Figure 2d**). Based on HOMA$_{IR}$ findings, intraperitoneal GTT (IP-GTT) and ITT (IP-ITT) were administered to determine the effect of the diets on glucose tolerance and insulin action. In line with weight gains, IP-GTT at 7 weeks on diets demonstrated that glucose intolerance and insulin resistance increased from SC<LFD<HFD<CAF (least resistant to most resistant) (**Figure 3a,b**), and insulin levels were significantly elevated for all diets relative to SC (**Figure 3c**). IP-ITT performed at 11 weeks on diets demonstrated that the insulin-mediated drop in glucose was not significantly different between diet exposures (**Figure 3d,e**).

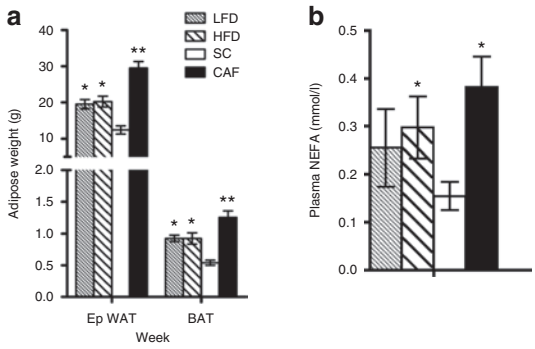

Figure 4 Dramatic increases in adiposity and nonesterified fatty acids (NEFAs) in cafeteria diet (CAF)-fed rats. (**a**) High-fat diet (HFD)-fed rats did not display differences in epididymal white adipose tissue (eWAT) or brown adipose tissue (BAT) size when compared to low-fat diet (LFD)-fed rats, but mass of both tissues was increased above standard chow (SC). CAF-fed animals had significantly larger eWAT and BAT fat pads compared to all groups (*P < 0.05 LF and HF vs. SC and CAF; **P < 0.05 CAF vs. all; n = 7–8, SC, LFD, and HFD, n = 10 CAF). (**b**) Similarly, CAF-fed rats displayed elevated circulating NEFA, with HFD and LFD groups displaying an intermediate level that were not statistically different between each other. (*P < 0.05 vs. SC; n = 4, SC, LFD, and HFD, n = 5 CAF).

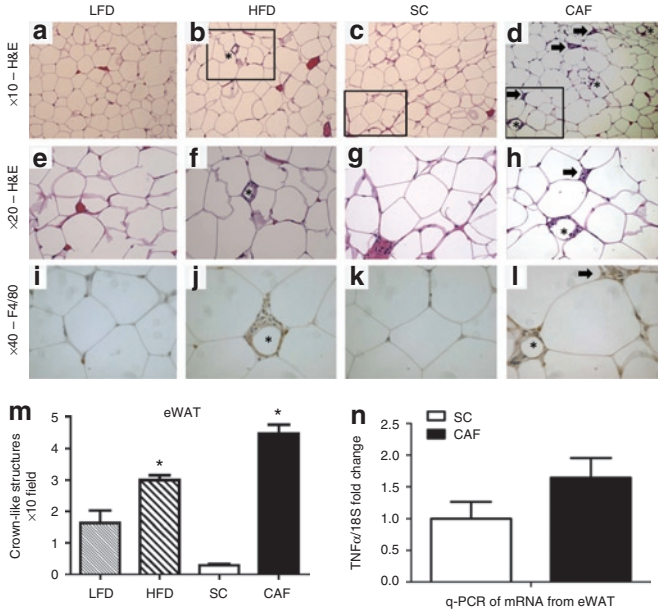

Figure 5 Epididymal white adipose tissue (eWAT) reveals dramatic macrophage infiltration and inflammation in cafeteria diet (CAF)-fed rodents. (**a**–**h**) ×10 and ×20 hematoxylin and eosin (H&E) stain of eWAT from (**a**,**e**) low-fat diet (LFD), (**b**,**f**) high-fat diet (HFD), (**c**,**g**) standard chow (SC), and (**d**,**h**) CAF. The box indicates areas of interest magnified to ×20 imaging when appropriate. Asterisks indicate crown-like structures (CLS), or areas of macrophage infiltration around adipocytes. Arrow indicates inflammatory loci. (**i**–**l**) Macrophage marker F4/80 was used to identify CLS (*) and areas of cells aggregating within inflammatory loci (arrow) (×40). (**m**) Quantification of CLS revealed a significant twofold increase in HFD- vs. LFD-fed adipose whereas CAF-fed adipose displayed a 17-fold increase over SC. (*CAF P < 0.05 vs. all, ^HFD P < 0.005 vs. all) (**n**) Pooled stromovascular fractions (SVF) from eWAT enriched in adipose-associated macrophages demonstrated higher expression of tumor necrosis factor α (TNFα) normalized to 18S in CAF-fed rats when compared to SC control animals as determined by qPCR. Representative images shown. (n = 4, SC, LFD, and HFD, n = 5 CAF). See **Supplementary Table S4** online for detailed description.

CAF-diet induced elevations in white and brown adipose mass, macrophage-containing CLS and inflammation

Obese humans with metabolic syndrome accumulate massive fat depots, which are shown to be chronically inflamed (18). To determine whether adiposity in the rodent models of obesity described here parallel physiologic indications of metabolic syndrome described above, we measured eWAT and BAT fat pad masses. CAF diet induced nearly a tripling of epididymal white and brown adipose mass compared to SC controls. HFD induced no change relative to LFD, but both were significantly different than SC and CAF (**Figure 4a**). Similar results were found for omental fat in an alternate set of animals after 10 weeks on experimental diets (data not shown). Elevations in plasma nonesterified fatty acids, another hallmark of metabolic syndrome, paralleled increased adipose mass with CAF diet exhibiting the highest levels of nonesterified fatty acids, which were significantly elevated over SC controls with LFD and HFD at intermediate concentrations (**Figure 4b**).

We next investigated the inflammatory status of eWAT since low-level chronic inflammation and macrophage infiltration into white adipose tissue is a well-documented phenomenon in animal and human obesity (18–20). Studies have shown that macrophages are necessary and sufficient to drive obesity and induce insulin resistance (15,21,22). Therefore, to examine whether CAF diet also induced macrophage infiltration in eWAT concurrent with increased fat pad size, detailed histologic analysis of eWAT was undertaken (**Figure 5**). Using macrophage marker F4/80, macrophage infiltration was substantially higher in CAF-fed eWAT compared to SC, LFD, and HFD-fed samples (**Figure 5i–l**). When compared to LFD controls, HFD-fed animals also displayed infiltrating macrophages although to a lesser extent than detected in CAF vs. SC. CLS are histological features found in obese adipose tissue and are demonstrated to be proinflammatory macrophages surrounding dying adipocytes, which are hallmarks of obese adipose (21). CAF diet induced a significant 14-fold increase in CLS over SC while a less than twofold increase was detected for HFD vs. LFD (**Figure 5m**). Likewise, dense areas of cell accumulation which stained positive for F4/80 were evident only in CAF-fed adipose. Weisberg *et al.* and Xu *et al.* demonstrated that macrophages present in the SVF contribute most of the inflammatory mediators in obese adipose tissue (17,23). Therefore, we focused our efforts on the dramatic CAF effects and isolated the SVF from SC and CAF eWAT fat pads. **Figure 5n** reports the quantification of tumor necrosis factor α mRNA expression in the SVF from SC control and CAF-fed rats, a proinflammatory cytokine well-established to induce insulin resistance in obese rodents and humans (24). Tumor necrosis factor α was elevated by 1.6-fold in the SVF isolated from CAF- vs. SC-fed eWAT, but did not reach statistical significance in this sample set.

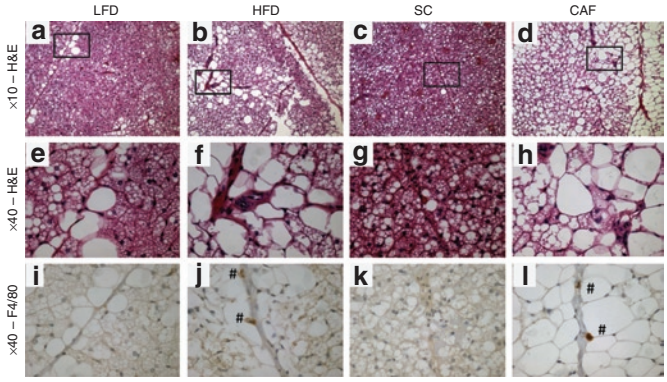

Figure 6 Brown adipose tissue (BAT) macrophage infiltration and lipid droplet accumulation is perivascular. (**a**–**h**) ×10 and ×40 hematoxylin and eosin (H&E) stain of BAT from (**a**,**e**) low-fat diet (LFD), (**b**,**f**) high-fat diet (HFD), (**c**,**g**) standard chow (SC), and (**d**,**h**) cafeteria diet (CAF). The box indicates area of the ×10 image magnified to ×40 imaging when appropriate for H&E stained tissues. Lipid droplet accumulation was notable in cells along the length of vessels in LFD, HFD, and especially CAF-fed tissues. (**i**–**l**) F4/80 was used to identify macrophages which can be seen as cells staining dark brown (marked with #) in (**j**) HFD and (**l**) CAF (×40). It is important to note that F4/80 positive macrophages colocalized to the perivascular regions where high lipid accumulation was noted and that CAF F4/80 positive cells stained stronger and were more numerous than those in HFD animals. Representative images are shown. (n = 4, SC, LFD, and HFD, n = 5 CAF). See **Supplementary Table S4** online for detailed description.

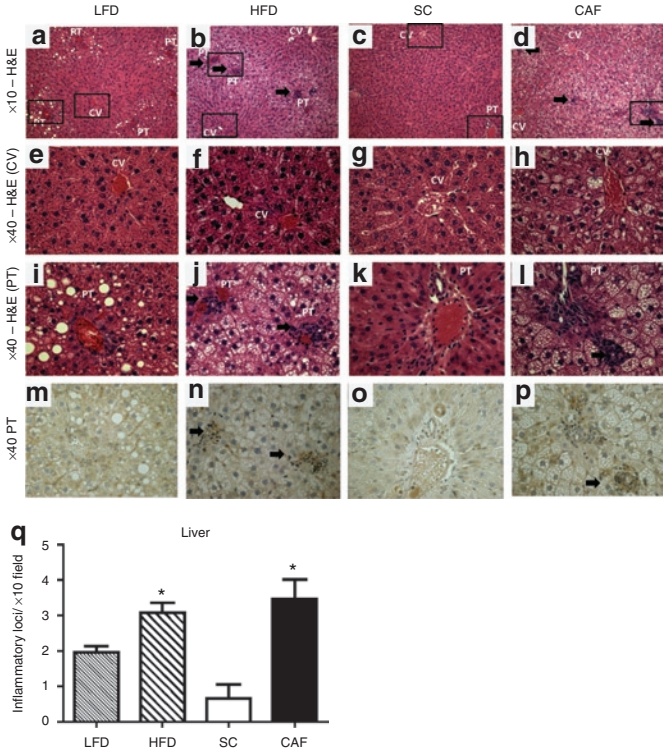

Figure 7 Histologic analysis of rat livers demonstrates dramatic macrophage infiltration and steatohepatitis in cafeteria diet (CAF)-fed rodents. (**a**–**l**) ×10 and ×40 hematoxylin and eosin (H&E) stain of liver from (**a**,**e**,**i**) low-fat diet (LFD), (**b**,**f**,**j**) high-fat diet (HFD), (**c**,**g**,**k**) standard chow (SC), and (**d**,**h**,**l**) CAF. Boxes indicate regions magnified to ×40 imaging when appropriate and arrows point to inflammatory loci. Central veins (CV; **e**–**h**) and portal triads (PT; **i**–**l**) are marked. Note healthy hepatic cord structure in (**c**) SC-fed livers when compared to macrovessicular steatosis in (**i**) LFD-fed livers and microvessicular steatotic livers in (**j**,**l**) HFD- and CAF-fed rodents. Lipid accumulation in LFD and HFD livers is localized to regions surrounding the (**i**,**j**) PT, leaving the (**e**,**f**) CV architecture intact, whereas in CAF-fed livers, lipid accumulation is (**h**,**l**) panlobular and the (**d**,**h**) hepatic cord architecture is disturbed. (**m**–**p**) Serial sections relating to images **i**–**l** which are stained using macrophage marker F4/80 identify areas of cells aggregating into inflammatory loci (arrows) around the PT in (**n**) HFD livers and (**p**) CAF livers (×40). Representative images are shown. (**q**) Quantification of inflammatory loci in livers revealed a significant 1.5-fold increase in HFD- vs. LFD-fed livers while CAF-fed livers displayed more than fivefold increase (*CAF and HFD $P < 0.05$ vs. SC). Data are presented as the mean ± s.e.m. (n = 4, SC, LFD, and HFD, n = 5 CAF). See **Supplementary Table S4** online for detailed description.

Little is known about macrophage infiltration into BAT other than increased macrophage infiltration of BAT in a transgenic lipodystrophy model (25). We investigated macrophage infiltration of BAT and indeed, compared to the normal architecture of SC-fed rats, increasing obesity causes enlarged fat droplets around vasculature in BAT with LFD and HFD amassing intermediate lipid droplets, and CAF diet inducing substantial fat accumulation. Only CAF-fed rats demonstrated large fat droplet accumulation in the BAT parenchyma extending from the vasculature (Figure 6a–h). This fat deposition is distinct from the WAT surrounding BAT on the periphery (data not shown). Both HFD and CAF diets induced strong F4/80 positive stained macrophages around the vessels, with elevations in CAF and HFD vs. SC and LFD controls (Figure 6i–l).

CAF-diet induced hepatosteatosis and inflammation

To investigate the effect of the human unhealthy food diet on the formation of nonalcoholic fatty liver disease (NAFLD), we evaluated serial sections of livers from each diet group. H&E staining of liver sections demonstrated normal liver structure in SC controls with some macrovessicular fat accumulation in LFD-fed rats. HFD and CAF-fed rat livers display minor to major microvessicular steatosis, respectively (Figure 7b and d, respectively). Steatosis associated with HFD was mixed macro- and microvesicular, localized to the periportal (Figure 7j) to midzonal regions and distinctly absent in the pericentral regions where normal tissue architecture was conserved (Figure 7f). Conversely, the CAF diet invoked hepatosteatosis that encompassed the entire liver lobule and was microvessicular in nature (Figure 7h,l). Next, we evaluated the ability of each diet to promote NASH by visually documenting F4/80 positive macrophage/Kupffer cell content and quantifying inflammatory loci, a collection of inflammatory cells primarily consisting of macrophages. LFD- and SC-fed rat livers displayed zero to very few inflammatory loci (Figure 7m,o, (respectively) and **q**). Although livers from rats fed HFD and CAF diets contained increased inflammatory loci vs. controls, there were dramatic differences in the size and localization of loci between HFD and CAF animals (Figure 7n,p, (respectively) and **q**). In livers from HFD-fed rats, F4/80 positive macrophages were small and limited to perivascular regions;

whereas loci from CAF-fed rats were found in both perivascular regions and within intralobular regions and were notably larger compared to HFD-fed animals (**Figure 7**).

CAF-diet induced islet dysfunction

Significantly elevated glucose and insulin levels and evidence of insulin resistance by GTT and ITT in the CAF animals led us to examine the pancreata by immunohistochemistry. LFD- and SC-fed rats displayed normal pancreatic islets with defined borders, whereas HFD-fed rats contained slightly hypertrophic and disfigured islets. Islets from CAF-fed rats were much larger in size, with dramatically distorted architecture (see **Supplementary Figure S2** online).

DISCUSSION

CAF: A model for human obesity and metabolic syndrome

DIO is a common tool used to examine metabolic syndrome in rodents. The study presented herein was a comprehensive physiologic and histologic analysis between a commonly used model for DIO (a lard-based HFD), an alternative dietary model of energy dense highly palatable cafeteria-style foods and controls fed LFD and SC. The CAF diet provides a highly relevant model in terms of examining the human diet in rodents and comes at a time when the poor eating habits of Americans are in the spotlight. Current worldwide increases in obesity cannot be accounted for by changes in genetic backgrounds alone. Therefore, diet combined with previous evolutionary selective pressure for a "thrifty," energy-conserving phenotype from when humans survived in a feast or famine world is an obvious contributing factor to this epidemic (26). Recent NHANES reports demonstrate that 33.6% of the American diet is comprised of fat (%kcal) (27). A study by the US Department of Agriculture on the US diet indicated that ~16% of Americans had overtly poor diets and that 74% needed to improve their diets, based on the US Department of Agriculture recommended daily allowances (RDA) for grains, vegetables, fruits, milk, meat, total fat, saturated fat, cholesterol, sodium, and dietary variety (28). Current research indicates that childhood obesity and dietary intake statistics also follow these trends. Increased snacking on energy dense foods parallels the dramatic increase in childhood obesity, with unhealthy snacks currently comprising >27% of an American child's daily caloric intake (29).

With these striking dietary trends in mind, we embarked on a study to examine a human diet in rodents compared to the traditional rodent diet most researchers use to model DIO. Our study has revealed that rats fed human nutrient-poor foods develop severe metabolic syndrome which is more robust than the effect of traditional HFD exposure. CAF-diet fed rats exhibited voluntary hyperphagia and grossly elevated fat intake which resulted in dramatic and rapid weight gain. Furthermore, CAF diet feeding promoted a prediabetic condition with elevated glucose, insulin, and nonesterified fatty acids, accompanied by decreased glucose and insulin tolerance. In addition, chronically inflamed liver and adipose tissues and distorted pancreatic islet architecture were prevalent.

Choice of control diet in animal studies

Interestingly, our results show that HFD did not induce a significant weight gain compared to LFD controls for up to 15 weeks of this diet. This suggests that either a longer diet is necessary to develop overt metabolic syndrome on the traditional high-fat lard-based diet or that the diet was started at an age that was too late to induce a divergent phenotype in our rats. It is likely that if we extended the study further or perhaps started in younger rats, a larger difference between the LFD and HFD could have emerged. An alternative explanation is that compared to standard chow SC, the LFD is very high in sucrose, with a simple exchange of fat for sugar to engineer the lard-based HFD. Indeed, compared to the SC, the LFD caused weight gain and moderate insulin resistance despite the fact that animals consumed relatively similar grams of food and fat calories. One reason could be that SC is undefined and contains carbohydrates derived from barley, oats, wheat, and corn rather than highly processed carbohydrate sources such as cornstarch, sucrose, and maltodextrin comprising the LFD diet. The whole-grains in SC contain phytoestrogens and high fiber which are protective against insulin resistance and obesity (30,31). In addition, the protein and fat sources vary between the SC groups. In sum, our varied results between SC and LFD chow "controls" demonstrate that chow diets vary widely in their effects, which emphasizes the relevance of chow sources and compositions, especially with respect to diet and obesity studies. A defined diet such as the LFD included in our study, which is commonly used as a control for HFD studies, is helpful in terms of knowing the composition but also has poor nutritional additives such as processed carbohydrates that can affect baseline measurements.

Interestingly, our study revealed that while HFD-fed animals decreased food intake in terms of total grams to maintain caloric intake comparable to LFD and SC control, CAF-fed animals lacked this autoregulatory mechanism. The highly palatable diet with varied flavors and textures seems to have disabled the normal homeostatic mechanism for energy balance possibly by activating the reward system (32). Energy-dense diets have been shown to alter normal appetite regulation (33,34). Another finding from this study is that nutritional components of the CAF diet have robust effects beyond the fat content alone. The CAF and HFD have similar fat contents at about 45–50% while their appropriate controls contained about 10–12% kcal derived from fat. Despite these relative similarities, the CAF-fed rats were hyperphagic, eating 40% more calories/day compared to the HFD. Although the CAF diet is high in fat, it is also high in sodium, saturated fatty acid, trans-fatty acids, and cholesterol and low in fiber and micronutrients such as vitamin A and calcium. All of these experimental components limit the interpretation of the CAF data such that no causal conclusions can be made as to the role or mechanism of a specific food component such as high-fat or high-sucrose exposure to weight gain associated with CAF diet. However, this experimental platform, which more accurately reflects early onset obesity and its associated pathologies, continues to be improved upon from its inception in 1982. Careful selection

of unhealthy food components with known nutritional content could facilitate a more mechanistic approach to understanding the relevant nutrients associated with rapid weight gain and progression toward disease states such as metabolic syndrome, NASH and type II diabetes.

Severe adipose and liver inflammation in CAF

Histologic analysis revealed that CAF-fed rats developed pathologic abnormalities in epididymal white adipose, brown adipose, liver, and pancreas consistent with metabolic syndrome. Chronic low-grade systemic inflammation is now considered to be a key component of metabolic syndrome with white adipose known to secrete many relevant adipokines (19,21). Visceral, not subcutaneous fat, is associated with metabolic syndrome in humans and rodents (35,36). It is well-established that macrophages infiltrate into obese adipose and are necessary and sufficient to perpetuate the obese state and insulin resistance (21). The CAF diet resulted in dramatic macrophage infiltration of eWAT and significantly increased the formation of CLS, hallmarks of inflammatory adipose. Histologic measures of inflammation were supported by quantitative PCR analysis of the macrophage-enriched SVF of eWAT that demonstrated increased expression of tumor necrosis factor α, a cytokine proven to be involved in insulin resistance and adipose lipolysis (24). In BAT, we discovered that large lipid droplets accumulate in the cells surrounding vessels, which correlated with weight gain in the LFD and HFD-fed rats, with CAF-fed BAT demonstrating the most profound lipid droplet accumulation. Importantly, this fat accumulation was distinct from any WAT that would be on the periphery of the BAT depot. Furthermore, we showed for the first time that the macrophage infiltration pattern of BAT differed from that of WAT. There were no CLS evident in BAT; however, infiltration of macrophages was detected in the perivascular region where large lipid droplet accumulation was prevalent. Currently, the role of perivascular macrophage accumulation in BAT is unclear.

Another contributing component of metabolic syndrome is fatty liver. NAFLD affects over one-third of the American population and ranges from hepatosteatosis to steatohepatitis, and could result in cirrhosis or hepatocellular carcinoma (37). NAFLD is strongly associated with visceral adiposity (38). Hepatosteatosis and steatohepatitis lead to liver insulin insensitivity and the inability to blunt gluconeogenesis, which is another contributing factor to metabolic syndrome (39). Our data indicate that SC rats have healthy livers with no steatosis or inflammation and histologically normal hepatic cords and other architecture. Hepatosteatosis developed in LFD livers with macrovessicular accumulations noted around the portal triad regions. In HFD livers, increased steatosis surrounding portal triads progressed to a microvessicular phenotype while the central vein architecture was preserved. The most extensive steatosis and distorted cord architecture was found in CAF-fed livers with microvessicular steatosis evident spanning from the portal triads to the central veins (panlobular). Macrosteatosis is thought to be benign and reversible while microsteatosis is considered malignant and precedes liver fibrosis (40). Prolonged steatosis can often lead to steatitis or activation of inflammatory cells in the liver. NAFLD, which is recognized as the hepatic manifestation of metabolic syndrome, is thought to occur in a two-hit manner with lipid accumulation followed by chronic inflammation, such as occurs with obesity (41). Like in adipose, it is thought that hepatosteatosis promotes the Th1 proinflammatory response suggesting that Kupffer cells could be polarized toward a proinflammatory phenotype, contributing to insulin resistance (42). Kupffer cells are resident liver macrophages and the primary source of liver inflammatory cytokines (41). Several groups have recently demonstrated that Kupffer cell activation is necessary to produce hepatic insulin resistance (42,43). Large Kupffer cells are thought to localize in the periportal zone and exhibit higher phagocytosis, protease activity, and inflammatory potential than smaller Kupffer cells in midzonal and pericentral regions (41). Interestingly, we detected numerous small loci of inflammatory cells present in HFD-fed livers, which accumulated around the portal triad regions. In the CAF-fed model however, inflammatory loci were larger and infiltrates were evident not only in the portal triad regions but also in the midzonal, intralobular regions. During steatosis, Kupffer cells display a diffuse localization whereas in NASH patients, Kupffer cells migrate to and aggregate around the pericentral regions (44). In the present study, the CAF liver phenotype with inflammatory loci both at the portal triads and within midzonal regions indicated macrophage migration from the portal triad to central vein and suggests the malignant progression from NAFLD to NASH.

Taken together, we have demonstrated in a comparative study that the CAF is a more robust model of metabolic syndrome than lard-based HFD and that the rapid-onset of weight gain, obesity, multiorgan dysfunctions and pathologies observed in the CAF model more closely reflect the modern human condition of early onset obesity. The CAF diet, while labor intensive and "untraditional," may be the best model to emulate modern human obesity trends.

SUPPLEMENTARY MATERIAL

Supplementary material is linked to the online version of the paper at http://www.nature.com/oby

ACKNOWLEDGMENTS

The project is funded by K99/R00 AA017376 to L.M. and a Freedom to Discover Award from Bristol Meyers Squibb to C.B.N. The funders had no role in study design, data collection and analysis, decision to publish, or preparation of the manuscript.

DISCLOSURE

The authors declared no conflict of interest.

REFERENCES

1. Flegal KM, Carroll MD, Ogden CL, Curtin LR. Prevalence and trends in obesity among US adults, 1999-2008. *JAMA* 2010;303:235–241.
2. Ogden CL, Carroll MD, Curtin LR, Lamb MM, Flegal KM. Prevalence of high body mass index in US children and adolescents, 2007-2008. *JAMA* 2010;303:242–249.
3. Klein JD, Dietz W. Childhood obesity: the new tobacco. *Health Aff (Millwood)* 2010;29:388–392.
4. Kennedy AJ, Ellacott KL, King VL, Hasty AH. Mouse models of the metabolic syndrome. *Dis Model Mech* 2010;3:156–166.

5. Rothwell NJ, Stock MJ. Combined effects of cafeteria and tube-feeding on energy balance in the rat. *Proc Nutr Soc* 1979;38:5A.
6. Sclafani A, Springer D. Dietary obesity in adult rats: similarities to hypothalamic and human obesity syndromes. *Physiol Behav* 1976;17:461–471.
7. Morris MJ, Chen H, Watts R, Shulkes A, Cameron-Smith D. Brain neuropeptide Y and CCK and peripheral adipokine receptors: temporal response in obesity induced by palatable diet. *Int J Obes (Lond)* 2008;32:249–258.
8. Caimari A, Oliver P, Keijer J, Palou A. Peripheral blood mononuclear cells as a model to study the response of energy homeostasis-related genes to acute changes in feeding conditions. *OMICS* 2010;14:129–141.
9. Heyne A, Kiesselbach C, Sahún I *et al*. An animal model of compulsive food-taking behaviour. *Addict Biol* 2009;14:373–383.
10. Rolls BJ, Rowe EA, Turner RC. Persistent obesity in rats following a period of consumption of a mixed, high energy diet. *J Physiol (Lond)* 1980;298:415–427.
11. Johnson PM, Kenny PJ. Dopamine D2 receptors in addiction-like reward dysfunction and compulsive eating in obese rats. *Nat Neurosci* 2010;13:635–641.
12. Shafat A, Murray B, Rumsey D. Energy density in cafeteria diet induced hyperphagia in the rat. *Appetite* 2009;52:34–38.
13. Muniyappa R, Chen H, Muzumdar R *et al*. Comparison between Surrogate Indexes of Insulin Sensitivity/Resistance and Hyperinsulinemic Euglycemic Clamp Estimates in Rats. *Am J Physiol Endocrinol Metab* 2009.
14. Cacho J, Sevillano J, de Castro J, Herrera E, Ramos MP. Validation of simple indexes to assess insulin sensitivity during pregnancy in Wistar and Sprague-Dawley rats. *Am J Physiol Endocrinol Metab* 2008;295:E1269–E1276.
15. Weisberg SP, Hunter D, Huber R *et al*. CCR2 modulates inflammatory and metabolic effects of high-fat feeding. *J Clin Invest* 2006;116:115–124.
16. Lee S, Muniyappa R, Yan X *et al*. Comparison between surrogate indexes of insulin sensitivity and resistance and hyperinsulinemic euglycemic clamp estimates in mice. *Am J Physiol Endocrinol Metab* 2008;294:E261–E270.
17. Weisberg SP, McCann D, Desai M *et al*. Obesity is associated with macrophage accumulation in adipose tissue. *J Clin Invest* 2003;112:1796–1808.
18. Rasouli N, Kern PA. Adipocytokines and the metabolic complications of obesity. *J Clin Endocrinol Metab* 2008;93:S64–S73.
19. Makowski L, Hotamisligil GS. Fatty acid binding proteins–the evolutionary crossroads of inflammatory and metabolic responses. *J Nutr* 2004;134:2464S–2468S.
20. Hotamisligil GS. Inflammation and endoplasmic reticulum stress in obesity and diabetes. *Int J Obes (Lond)* 2008;32 Suppl 7:S52–S54.
21. Anderson EK, Gutierrez DA, Hasty AH. Adipose tissue recruitment of leukocytes. *Curr Opin Lipidol* 2010;21:172–177.
22. Furuhashi M, Fucho R, Görgün CZ *et al*. Adipocyte/macrophage fatty acid-binding proteins contribute to metabolic deterioration through actions in both macrophages and adipocytes in mice. *J Clin Invest* 2008;118:2640–2650.
23. Xu H, Barnes GT, Yang Q *et al*. Chronic inflammation in fat plays a crucial role in the development of obesity-related insulin resistance. *J Clin Invest* 2003;112:1821–1830.
24. Sethi JK, Hotamisligil GS. The role of TNF alpha in adipocyte metabolism. *Semin Cell Dev Biol* 1999;10:19–29.
25. Herrero L, Shapiro H, Nayer A, Lee J, Shoelson SE. Inflammation and adipose tissue macrophages in lipodystrophic mice. *Proc Natl Acad Sci USA* 2010;107:240–245.
26. Prentice AM, Rayco-Solon P, Moore SE. Insights from the developing world: thrifty genotypes and thrifty phenotypes. *Proc Nutr Soc* 2005;64:153–161.
27. US Department of Agriculture ARS. *Nutrient Intake From Food: Mean Amounts Consumed Per Individual, One Day, 2005–2006*. 2008.
28. Basiotis PP, Carlson A, Gerrior SA, Juan WY, Lino M. The Healthy Eating Index: 1999–2000. United States Department of Agriculture Center for Nutrition Policy and Promotion, 2002.
29. Piernas C, Popkin BM. Trends in snacking among U.S. children. *Health Aff (Millwood)* 2010;29:398–404.
30. Bhathena SJ, Velasquez MT. Beneficial role of dietary phytoestrogens in obesity and diabetes. *Am J Clin Nutr* 2002;76:1191–1201.
31. Isken F, Klaus S, Osterhoff M, Pfeiffer AF, Weickert MO. Effects of long-term soluble vs. insoluble dietary fiber intake on high-fat diet-induced obesity in C57BL/6J mice. *J Nutr Biochem* 2010;21:278–284.
32. Saper CB, Chou TC, Elmquist JK. The need to feed: homeostatic and hedonic control of eating. *Neuron* 2002;36:199–211.
33. Erlanson-Albertsson C. How palatable food disrupts appetite regulation. *Basic Clin Pharmacol Toxicol* 2005;97:61–73.
34. Rolls BJ. The relationship between dietary energy density and energy intake. *Physiol Behav* 2009;97:609–615.
35. Després JP. Is visceral obesity the cause of the metabolic syndrome? *Ann Med* 2006;38:52–63.
36. Bruun JM, Lihn AS, Pedersen SB, Richelsen B. Monocyte chemoattractant protein-1 release is higher in visceral than subcutaneous human adipose tissue (AT): implication of macrophages resident in the AT. *J Clin Endocrinol Metab* 2005;90:2282–2289.
37. Park EJ, Lee JH, Yu GY *et al*. Dietary and genetic obesity promote liver inflammation and tumorigenesis by enhancing IL-6 and TNF expression. *Cell* 2010;140:197–208.
38. Francque S, Verrijken A, Mertens I *et al*. Visceral adiposity and insulin resistance are independent predictors of the presence of non-cirrhotic NAFLD-related portal hypertension. *Int J Obes (Lond)* 2010.
39. van der Poorten D, Milner KL, Hui J *et al*. Visceral fat: a key mediator of steatohepatitis in metabolic liver disease. *Hepatology* 2008;48:449–457.
40. Burt AD, Mutton A, Day CP. Diagnosis and interpretation of steatosis and steatohepatitis. *Semin Diagn Pathol* 1998;15:246–258.
41. Baffy G. Kupffer cells in non-alcoholic fatty liver disease: the emerging view. *J Hepatol* 2009;51:212–223.
42. Kremer M, Hines IN, Milton RJ, Wheeler MD. Favored T helper 1 response in a mouse model of hepatosteatosis is associated with enhanced T cell-mediated hepatitis. *Hepatology* 2006;44:216–227.
43. Lanthier N, Molendi-Coste O, Horsmans Y *et al*. Kupffer cell activation is a causal factor for hepatic insulin resistance. *Am J Physiol Gastrointest Liver Physiol* 2010;298:G107–G116.
44. Lefkowitch JH, Haythe JH, Regent N. Kupffer cell aggregation and perivenular distribution in steatohepatitis. *Mod Pathol* 2002;15:699–704.